

Article

Pressure Effect on Elastic Constants and Related Properties of Ti_3Al Intermetallic Compound: A First-Principles Study

Xianshi Zeng ¹, **Rufang Peng** ², **Yanlin Yu** ³, **Zuofu Hu** ³, **Yufeng Wen** ^{3,*} and **Lin Song** ⁴ 

¹ Research Center of Laser Fusion, China Academy of Engineering Physics, Mianyang 621900, China; zengxueliang@163.com

² State Key Laboratory for Environment-Friendly Energy Materials, Southwest University of Science and Technology, Mianyang 621010, China; rfpeng2006@163.com

³ School of Mathematical Sciences and Physics, Jinggangshan University, Ji'an 343009, China; yuyanlin_121@163.com (Y.Y.); huzuofu@outlook.com (Z.H.)

⁴ State Key Laboratory of Solidification Processing, Northwestern Polytechnical University, Xi'an 710072, China; songlin@nwpu.edu.cn

* Correspondence: jgsuwfy@sina.com; Tel.: +86-796-810-0488

Received: 30 August 2018; Accepted: 11 October 2018; Published: 17 October 2018



Abstract: Using first-principles calculations based on density functional theory, the elastic constants and some of the related physical quantities, such as the bulk, shear, and Young's moduli, Poisson's ratio, anisotropic factor, acoustic velocity, minimum thermal conductivity, and Debye temperature, are reported in this paper for the hexagonal intermetallic compound Ti_3Al . The obtained results are well consistent with the available experimental and theoretical data. The effect of pressure on all studied parameters was investigated. By the mechanical stability criteria under isotropic pressure, it is predicted that the compound is mechanically unstable at pressures above 71.4 GPa. Its ductility, anisotropy, and Debye temperature are enhanced with pressure.

Keywords: Ti_3Al intermetallic compound; elastic properties; high pressure; first-principles calculations

1. Introduction

Elastic constants are very important quantities to describe the mechanical properties of materials. They are evidently and directly employed to evaluate the elastic strains or energies in materials under stress of various origins: external, internal, thermal, etc. The plastic properties of materials are closely correlated with the shear moduli along the slip planes of mobile dislocations since these dislocations can dissociate into partials with a spacing determined by the balance between the planar fault energy and the repulsive elastic force [1]. Values of elastic constants provide valuable information on the structural stability, the bonding characteristic between adjacent atomic planes, and the anisotropic character of the bonding [1]. Elastic properties are also closely associated with many fundamental solid-state properties, such as acoustic velocity, thermal conductivity, Debye temperature, interatomic potentials, and so on.

The intermetallic titanium aluminides Ti_3Al and $TiAl$ are promising high-temperature structural materials for engine and airframe applications due to their low density and excellent high-temperature properties [2]. However, one main technological problem is to improve the room-temperature ductility of Ti_3Al and $TiAl$ for their practical use. It is well known that the crystal structure of a material plays a crucial role in determining its ductility. The ductility of the Ti_3Al intermetallic compound is mainly attributed to the hexagonal crystal structure of the Ni_3Sn -type DO_{19} with a limited number of available activated slip systems and the covalent bonding between the constituent elements. The slip on the

(100) prism plane can be activated in DO_{19} Ti_3Al while the slip on the (001) basal plane is seldom observed due to a high critical resolved shear stress [3]. On the other hand, alloys based on the TiAl intermetallic compound with a good balance of higher strength and better ductility generally possess dual-phase lamellar structures composed mainly of the $\text{L}1_0$ -ordered tetragonal TiAl (γ) phase and a small amount of the hexagonal Ti_3Al (α_2) phase [4]. The anisotropy of the deformation mode of the α_2 phase strongly affects the plastic behavior of dual-phase alloys and, thus, the control of the plastic anisotropy of the α_2 phase holds the key to improving the ductility of the alloys [5]. The growing interest in dual-phase alloys further encourages our interest in the intermetallic compound Ti_3Al .

It is known that pressure is a key variable to tune a material's solid-state properties. Nevertheless, only a few studies on the properties of Ti_3Al under pressure have been carried out, to the best of our knowledge. Using the technique of high-pressure X-ray diffraction, Sahu et al. revealed that pressure in the range of 10–15 GPa induces the original Ni_3Sn -type DO_{19} structure of Ti_3Al to transform into the Ni_3Ti -type DO_{24} one [6]. Subsequently, Rajaopalan et al. confirmed the pressure-induced phase transition in Ti_3Al using first-principles calculations with the tight-binding linear muffin-tin orbital (TB-LMTO) method [7]. However, Dubrovinskaia et al. investigated in detail the behavior of Ti_3Al with various Al content at pressures up to 25 GPa by means of high-pressure *in situ* powder X-ray diffraction and first-principles calculations with linear muffin-tin orbital atomic-sphere (LMTO-ASA) and full-potential linear muffin-tin orbital (FP-LMTO) methods [8]. They revealed there was no pressure-induced structural phase transition in Ti_3Al up to 25 GPa. Thereafter, Zhang et al. studied the structural, elastic, and thermodynamic properties of Ti_3Al under pressure up to 30 GPa using first-principles calculations based on density functional theory (DFT) and ultrasoft pseudo-potential (USPP) methods [9]. They found that the hexagonal structure of Ti_3Al is elastically stable in the pressure range of 0–30 GPa, and the pressure can improve its ductility.

To gain a deeper understanding of the high-pressure properties for Ti_3Al , in the present work, we focus on studying the elastic constants and some properties related to these constants for this compound in the range of 0–80 GPa by first-principles calculations based on DFT and projector augmented wave (PAW) methods.

2. Theoretical Methods

2.1. Computational Details

All the calculations based on DFT were carried out using the Vienna Ab initio Simulation Package (VASP, version 5.4) [10–12]. The ion–electron interaction is described by the PAW method [13,14]. The exchange-correlation functional is treated with the Perdew, Burke, and Ernzerhof (PBE) generalized gradient approximation (GGA) [15,16]. The valence electron configurations for Ti and Al correspond to $3s^23p^63d^24s^2$ and $3s^23p^1$. The plane wave cut-off energy was set as 600 eV. A convergence criterion of 10^{-6} eV/atom was used for the electronic self-consistency loop. The k -point meshes for the Brillouin zone sampling was constructed through the Monkhorst-Pack scheme [17]. An $11 \times 11 \times 13$ k -points grid was used. Before calculating the elastic constants of the Ti_3Al intermetallic compound at a given pressure P , the unit cell of the compound at the corresponding pressure was optimized by full relaxation with respect to the volume, shape, and internal atomic positions until the atomic forces were less than 10^{-2} eV/Å.

2.2. Calculations of Elastic Constants

The number of independent single-crystal elastic constants is five for the hexagonal intermetallic compound Ti_3Al , i.e., C_{11} , C_{12} , C_{13} , C_{33} , and C_{44} . Starting from the optimized unit cells under different pressures, in this study, we used the strain–stress relationship method to determine all five elastic constants, as implemented in the VASP [18]. The elastic constants are defined as the first derivatives of the stresses with respect to the strain tensor. The elastic tensor was determined by performing six finite distortions of the lattice and deriving the elastic constants from the strain–stress

relationship [19]. The elastic tensor was calculated for rigid ions, as well as allowing for relaxation of the ions. The ionic contributions were determined by inverting the ionic Hessian matrix and multiplying with the internal strain tensor [20]. The final elastic constants include both the contributions from distortions with rigid ions and the contributions from the ionic relaxations.

3. Results and Discussion

3.1. Bulk Properties at Zero Pressure

The crystal structures of the hexagonal intermetallic compound Ti_3Al are shown in Figure 1. There are a total of eight atoms in the unit cell of the compound. Among these atoms, six Ti atoms occupy 6 h Wyckoff positions and two Al atoms occupy 2c Wyckoff positions. Experimentally, the single-crystal elastic constants of Ti_3Al have been measured by Tanaka and Koiwa [21] using the rectangular parallelepiped resonance method. Theoretically, the elastic properties of Ti_3Al have been investigated by Zhang et al. [9], Wei et al. [22], and Liu et al. [23] with the USPP and the GGA methods, by Music and Schneider [24] with the PAW and the GGA methods, and by Fu et al. [25] with the full-potential linearized augmented plane-wave (FLAPW) and the local density approximation (LDA) methods. Table 1 presents the ground-state equilibrium lattice parameter and the elastic constants of the Ti_3Al intermetallic compound in comparison with reported experimental data [21,26] and other theoretical values [9,22–25]. Comparison of the lattice parameters a and c/a shows that the present results are well consistent with the available experimental and theoretical results. The c/a ratio of 0.808 is correctly predicted in this study and fits well with the experimental value of 0.80. The presently obtained elastic constants are in good agreement with the experimental data [21], exhibiting smaller deviations as compared to the other theoretical results [9,22–25]. These indicate that the present calculation conditions are sufficiently reliable. Moreover, the mechanical stability conditions for hexagonal crystals at 0 GPa are as follows [27]:

$$C_{44} > 0, \quad C_{11} - |C_{12}| > 0, \quad C_{33}(C_{11} + C_{12}) - 2C_{13}^2 > 0 \quad (1)$$

These conditions are associated with different deformations of the crystals. A value approaching zero indicates the shear deformation of the cell for C_{44} , the expansion of the direction along the spindle axis during the contraction of the other symmetry direction perpendicular to the spindle axis for $C_{11} - |C_{12}|$, and the deformation of the volume for $C_{33}(C_{11} + C_{12}) - 2C_{13}^2$. The elastic constants of Ti_3Al obtained in this study satisfy the three conditions above, which shows that its hexagonal structure is mechanically stable at zero pressure.

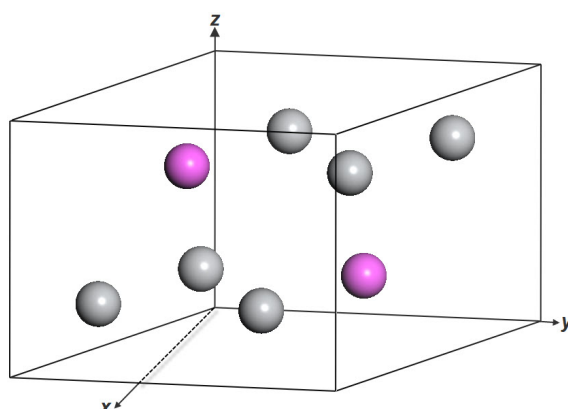


Figure 1. Crystal structure of Ti_3Al .

Table 1. The optimized lattice parameters a (in Å), c/a , and elastic constants (in GPa) of Ti_3Al at zero pressure.

	a	c/a	C_{11}	C_{12}	C_{13}	C_{33}	C_{44}
Present	5.758	0.808	186.18	85.57	62.76	233.03	59.75
Exp. [21,26]	5.77	0.80	183.2	89.0	62.6	225.1	64.1
Theo. [22]	5.74	0.81	184.67	82.37	63.41	225.08	53.97
Theo. [24]	5.772	0.803					72
Theo. [9]	5.76	0.809	192.2	80.5	62.5	232.9	61.6
Theo. [23]	5.72	0.81	185	83	63	231	57
Theo. [25]	5.64	0.81	221	71	85	238	69

3.2. Pressure-Dependent Structure Parameters

Figure 2 shows the pressure dependence of the lattice constant ratio c/a , the normalized lattice parameters a/a_0 , c/c_0 , and the normalized volume V/V_0 of Ti_3Al , where a_0 , c_0 , and V_0 are the optimized lattice constants and volume at 0 GPa, respectively. The slight increase of the value for c/a with pressure in the figure indicates the better resistance to compression along the c axis. Meanwhile, the values of a/a_0 , c/c_0 , and V/V_0 monotonically decrease with pressure. The normalized parameter a/a_0 changes more rapidly than the counterpart c/c_0 . At same pressure, the value of a/a_0 is always smaller than that of c/c_0 . These also indicate the better resistance to compression along the c axis.

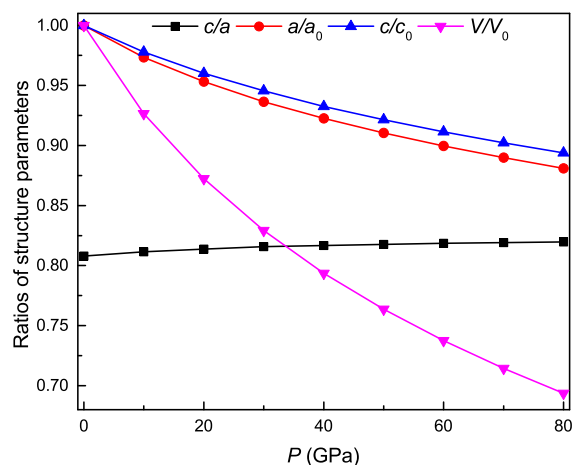


Figure 2. The ratios of structural parameters as a function of pressure for Ti_3Al .

3.3. Pressure-Dependent Elastic Constants and Mechanical Properties

The calculated results of the elastic constant for Ti_3Al under different pressures are presented in Table 2. The elastic constants C_{11} and C_{33} represent the elasticity in length. The other constants C_{12} , C_{13} , and C_{44} are associated with the elasticity in shape. One can find that the four elastic constants for the hexagonal Ti_3Al increase monotonically with pressure except for C_{44} . The constants C_{11} and C_{33} change rapidly with pressure, C_{12} and C_{13} change moderately under pressure, while C_{44} incipiently increases slightly with pressure up to 40 GPa and then decreases gently under higher pressure. One can also find that the elastic constant C_{11} is always smaller than the counterpart C_{33} at the same pressure, showing that it is easier to compress along the [100] direction than along the [001] direction. Moreover, for hexagonal crystals, the conditions of mechanical stability under isotropic pressure are given by [28]

$$\tilde{C}_{44} > 0, \quad \tilde{C}_{11} - |\tilde{C}_{12}| > 0, \quad \tilde{C}_{33}(\tilde{C}_{11} + \tilde{C}_{12}) - 2\tilde{C}_{13}^2 > 0 \quad (2)$$

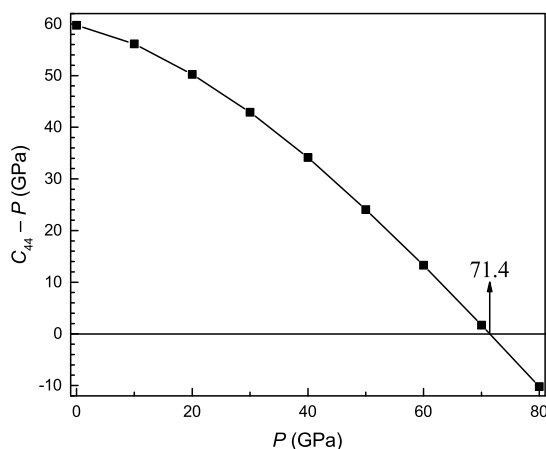
with

$$\tilde{C}_{ii} = C_{ii} - P \quad (i = 1, 3, 4), \quad \tilde{C}_{12} = C_{12} + P, \quad \tilde{C}_{13} = C_{13} + P \quad (3)$$

Table 2. The elastic constants C_{ij} (in GPa) of Ti_3Al under pressure up to 80 GPa.

P	C_{11}	C_{12}	C_{13}	C_{33}	C_{44}
0	186.18	85.57	62.76	233.03	59.75
10	224.30	108.15	75.51	286.13	66.15
20	261.44	124.83	89.61	323.41	70.22
30	291.09	142.23	105.72	354.83	72.90
40	318.32	157.86	122.34	380.17	74.16
50	343.06	174.27	135.46	402.06	74.06
60	366.48	191.39	149.52	430.75	73.29
70	389.37	208.75	161.36	460.66	71.69
80	409.54	228.60	172.83	492.29	69.81

The three conditions are related to different deformations of the crystals under isotropic pressure. A value approaching zero indicates the shear deformation of the cell under isotropic pressure for \tilde{C}_{44} , the expansion of the direction along the spindle axis under isotropic pressure during the contraction of the other symmetry direction perpendicular to the spindle axis under isotropic pressure for $\tilde{C}_{11} - |\tilde{C}_{12}|$, and the deformation of the volume under isotropic pressure for $\tilde{C}_{33}(\tilde{C}_{11} + \tilde{C}_{12}) - 2\tilde{C}_{13}^2$. Figure 3 shows the pressure dependence of \tilde{C}_{44} for the Ti_3Al intermetallic compound. When the value of \tilde{C}_{44} is no longer larger than zero, it indicates that the hexagonal structure of the compound is mechanically unstable above pressures of about 71.4 GPa.

**Figure 3.** The constant $C_{44} - P$ as a function of pressure for Ti_3Al .

Sahu et al. [6] performed high-pressure X-ray diffraction studies of Ti_3Al , and revealed a phase transition from the DO_{19} to DO_{24} structure in the pressure range of 10–15 GPa. Then, Rajaopalan et al. [7] theoretically confirmed the finding by taking the TB-LMTO approach within the atomic-sphere approximation (ASA) and the LDA. Dubrovinskaia et al. [8] pointed out that the high-pressure study in Ref. [6] was conducted on one single sample, and the interpretation of the results was not unambiguous, in addition to the fact that the calculations reported in Ref. [7] were conducted within the so-called ASA, which sometimes fails to resolve small structural energy differences. Thus, they performed a series of experiments on a number of samples with different compositions of Ti_3Al by means of high-pressure in situ powder X-ray diffraction, and theoretically complemented them by using the LMTO-ASA method with the coherent potential approximation (CPA), and the FP-LMTO method with the GGA [8]. In their study, neither experiment nor theory observed the pressure-induced phase transition from the DO_{19} to the DO_{24} structure under pressure conditions of up to 25 GPa, and the possible reasons for the difference between their experimental study results and those of Sahu et al. [6] were also analyzed in detail. Zhang et al. [9] studied the structural stability of Ti_3Al under pressures up to 30 GPa with the USPP and the GGA methods and found that the DO_{19} structure of Ti_3Al is mechanically stable in the

pressure range of 0–30 GPa. The result of our theoretical study agrees with that of the experimental and theoretical study in Ref. [8] and the theoretical study in Ref. [9].

From the obtained constants C_{ij} s of a single crystal, the bulk modulus (B) and shear modulus (G) of the polycrystal materials can be calculated by the Voigt–Reuss–Hill (VRH) approximation [29–31]. For the hexagonal structure, the bulk and shear moduli in the VRH approximation are given by

$$B = \frac{B_V + B_R}{2}, \quad G = \frac{G_V + G_R}{2} \quad (4)$$

where B_V and G_V correspond to Voigt's bulk modulus and shear modulus, B_R and G_R are Reuss's bulk modulus and shear modulus, respectively, and they are given by [32,33]

$$\begin{aligned} B_V &= \frac{2C_{11} + 2C_{12} + 4C_{13} + C_{33}}{9}, \quad G_V = \frac{C_{11} + C_{12} - 4C_{13} + 2C_{33} + 12C_{44} + 12C_{66}}{30}, \\ B_R &= \frac{(C_{11} + C_{12})C_{33} - 2C_{13}^2}{C_{11} + C_{12} - 4C_{13} + 2C_{33}}, \quad G_R = \frac{5[(C_{11} + C_{12})C_{33} - 2C_{13}^2]C_{44}C_{66}}{6B_V C_{44}C_{66} + 2[(C_{11} + C_{12})C_{33} - 2C_{13}^2](C_{44} + C_{66})} \end{aligned} \quad (5)$$

with

$$C_{66} = \frac{C_{11} - C_{12}}{2} \quad (6)$$

Further, the Young's modulus (E) and Poisson's ratio (ν) are estimated by [29–31]

$$E = \frac{9BG}{3B + G}, \quad \nu = \frac{3B - 2G}{6B + 2G} \quad (7)$$

Figure 4 shows the pressure dependence of bulk, shear, and Young's moduli and Poisson's ratio for the Ti_3Al intermetallic compound. The bulk modulus reflects the resistance of materials against volume change. The shear modulus reflects the resistance of materials against shape change. The Young's modulus measures the stiffness of materials, and the larger its value, the stiffer the material. From Figure 4, it is clearly seen that the values of B , G , and E increase monotonously with pressure, and the change trend is linear for B while nonlinear for G and E . These results mean that the volume change resistance increases linearly, while the shape change resistance and stiffness increase nonlinearly with pressure. Our calculated bulk, shear, and Young's moduli at zero pressure are 114.04, 59.33, and 151.69 GPa, respectively, which are in excellent agreement with the corresponding experimental data of 113, 59, and 151 GPa [21]. Meanwhile, our calculated zero-pressure bulk modulus is also in excellent agreement with the theoretical values of 114 GPa [22] and 112.54 GPa [24].

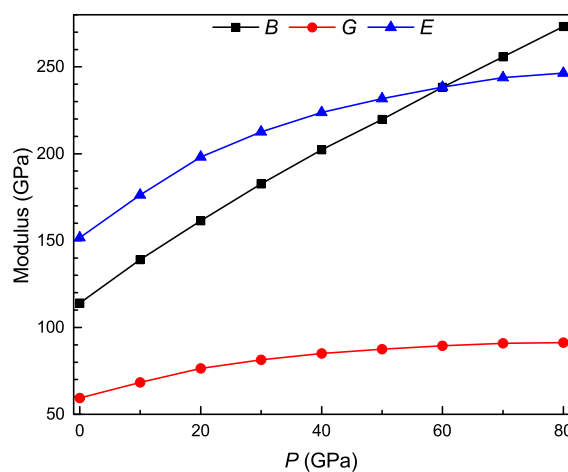


Figure 4. Bulk (B), shear (G), and Young's (E) moduli as a function of pressure for Ti_3Al .

For the specific case of hexagonal crystals, the Cauchy pressure is defined as $(C_{13} - C_{44})$ for (100) plane and $(C_{12} - C_{66})$ for the (001) plane. Figure 5 shows the pressure dependence of the B/G ratio, Poisson's ratio, and Cauchy pressures for the Ti_3Al intermetallic compound. These quantities allow us to assess the ductility/brittleness of materials. According to Pugh's rule [34], the high and low values of B/G are related to ductility and brittleness, respectively. Ductile behavior is exhibited in materials when $B/G > 1.75$, otherwise the materials behave in a brittle manner. As shown in Figure 5a, the B/G ratio increases monotonically with pressure, which is always more than 1.75 in the studied pressure range. These indicate that Ti_3Al becomes more ductile with pressure. According to the rule proposed by Frantsevich et al. [35], a brittle behavior is exhibited in materials when $\nu < 0.26$, otherwise the materials behave in a ductile manner. As shown in Figure 5b, Poisson's ratio also increases monotonically with pressure, which is always more than 0.26 in the studied pressure range. These also indicate that Ti_3Al becomes more ductile with pressure. According to Pettifor's rule [36], the materials with larger positive Cauchy pressures have more metallic bonds and thus become more ductile, otherwise the Cauchy pressures of the materials are more negative, they have more angular bonds, and thus exhibit more brittleness. As shown in Figure 5c,d, the increase of positive values for both Cauchy pressures with pressure indicate that there is more metallic bonding in Ti_3Al with pressure, and thus it becomes more ductile. At the same pressure, the Cauchy pressure $(C_{12} - C_{66})$ is always larger than the counterpart $(C_{13} - C_{44})$, implying that the metallic character of the bonding in the (001) plane is more significant than that in the (100) plane. Hardness is a measure of the resistance to elastic deformation, plastic deformation, or failure under external force; these are dependent on elastic constants, plasticity, strain, ductility, strength, etc. Theoretically, the hardness (H) of polycrystalline materials can be estimated by [37]

$$H = 2\left(\frac{G^3}{B^2}\right)^{0.585} - 3 \quad (8)$$

The pressure dependence of theoretical hardness is shown in Figure 6. It is clearly observed that the hardness decreases approximately with pressure.

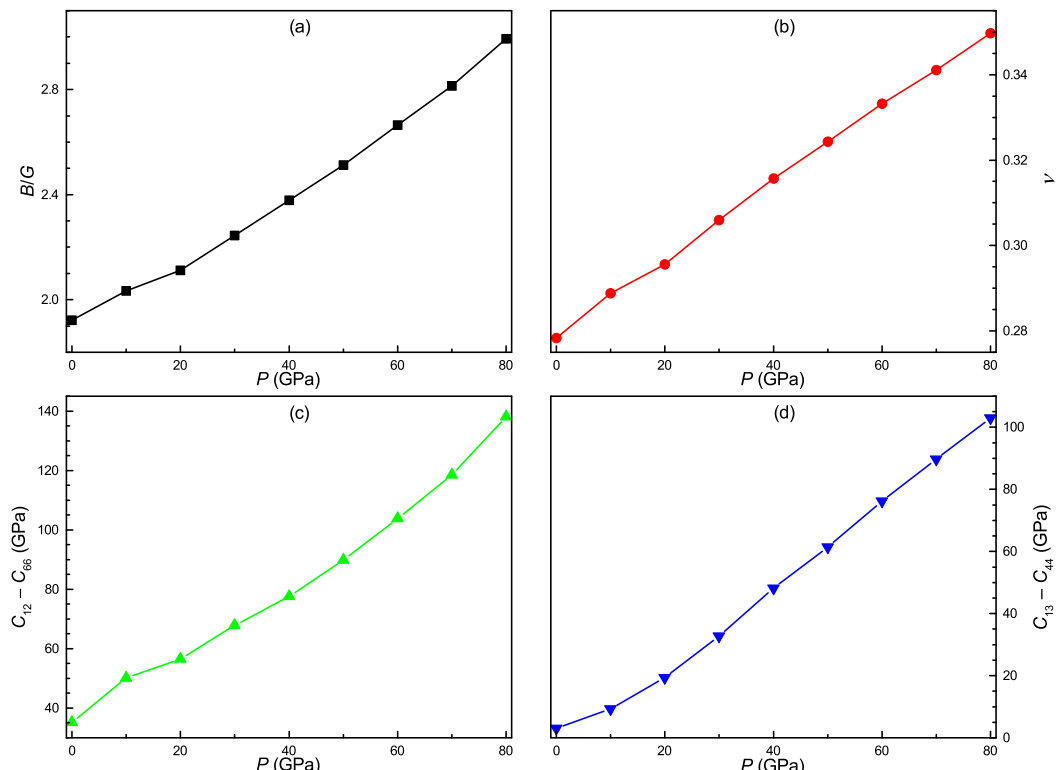


Figure 5. B/G ratio (a), Poisson's ratio (b), and Cauchy pressures $C_{12} - C_{66}$ (c), $C_{13} - C_{44}$ (d) as a function of pressure for Ti_3Al .

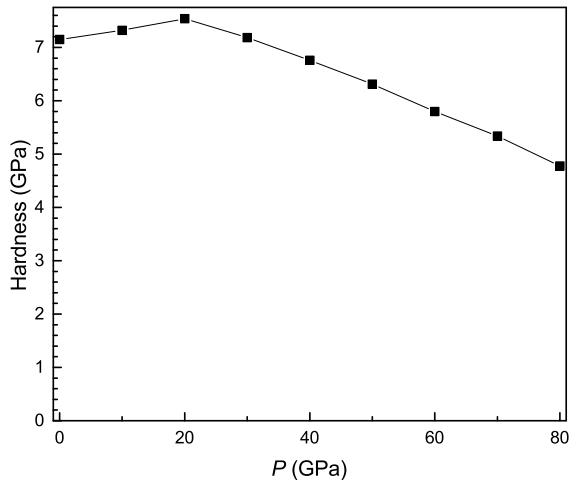


Figure 6. Hardness as a function of pressure for Ti₃Al.

3.4. Pressure-Dependent Elastic Anisotropy

In material science, elastic anisotropy is the directional dependence of the physical properties of materials. Most materials exhibit elastically anisotropic behavior. Some examples are the directional dependence of the bulk modulus, Young's modulus, shear modulus, and Poisson's ratio. For hexagonal system, the linear bulk modulus along the *a* and *c* principle axes (B_a and B_c) are given by [38]

$$B_a = a \frac{dP}{da} = \frac{\lambda}{2 + \alpha}, \quad B_c = c \frac{dP}{dc} = \frac{B_a}{\alpha} \quad (9)$$

with

$$\lambda = 2(C_{11} + C_{12}) + 4C_{13}\alpha + C_{33}\alpha^2, \quad \alpha = \frac{C_{11} + C_{12} - 2C_{13}}{C_{33} - C_{13}} \quad (10)$$

where α also signifies the anisotropy of linear compressibility along the *a* or *c* axis. For an isotropic material, the value of α must be unity. A deviation less than or greater than unity represents the degree of anisotropy. As shown in Figure 7b, Ti₃Al presents elastic anisotropy due to its α being a value smaller than unity. The values of α increase approximately with pressure, but the variation is very small.

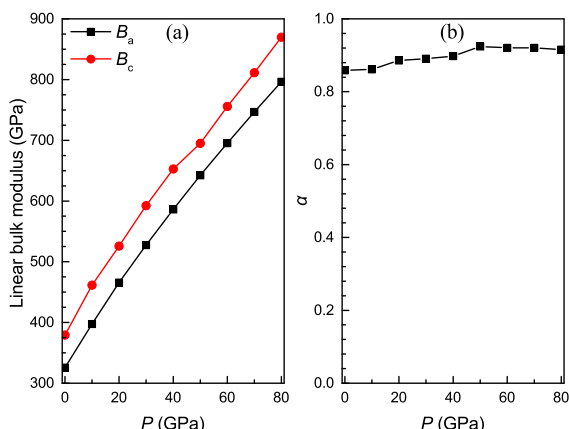


Figure 7. Linear bulk modulus along the *a* and *c* principle axes (a) and its anisotropy α (b) as a function of pressure for Ti₃Al.

The average Young's modulus on the (2̄10) and (010) prismatic planes and the (001) basal plane ($E_{(2\bar{1}0)}$, $E_{(010)}$, and $E_{(001)}$) are given by [30,39]

$$E_{(2\bar{1}0)} = E_{(010)} = \frac{1}{S_{11}}, \quad E_{(001)} = \frac{1}{S_{33}} \quad (11)$$

with

$$S_{11} = \frac{1}{2} \left[\frac{C_{33}}{C_{33}(C_{11} + C_{12}) - 2C_{13}^2} + \frac{1}{C_{11} - C_{12}} \right], \quad S_{33} = \frac{C_{11} + C_{12}}{C_{33}(C_{11} + C_{12}) - 2C_{13}^2} \quad (12)$$

The average shear modulus on the $(2\bar{1}0)$ and (010) prismatic planes and the (001) basal plane ($G_{(2\bar{1}0)}$, $G_{(010)}$, and $G_{(001)}$) are given by [30,39]

$$G_{(2\bar{1}0)} = G_{(010)} = \frac{2}{2(S_{11} - S_{12}) + S_{44}}, \quad G_{(001)} = \frac{1}{S_{44}} \quad (13)$$

with

$$S_{11} - S_{12} = \frac{1}{C_{11} - C_{12}}, \quad S_{44} = \frac{1}{C_{44}} \quad (14)$$

The average Poisson's ratio on the $(2\bar{1}0)$ and (010) prismatic planes and the (001) basal plane ($\nu_{(2\bar{1}0)}$, $\nu_{(010)}$, and $\nu_{(001)}$) are given by [30,39]

$$\nu_{(2\bar{1}0)} = \nu_{(010)} = -\frac{S_{12} + S_{13}}{2S_{11}}, \quad \nu_{(001)} = -\frac{S_{13}}{S_{33}} \quad (15)$$

with

$$\begin{aligned} S_{11} &= \frac{1}{2} \left[\frac{C_{33}}{C_{33}(C_{11} + C_{12}) - 2C_{13}^2} + \frac{1}{C_{11} - C_{12}} \right], \\ S_{12} &= \frac{1}{2} \left[\frac{C_{33}}{C_{33}(C_{11} + C_{12}) - 2C_{13}^2} - \frac{1}{C_{11} - C_{12}} \right], \\ S_{13} &= -\frac{C_{13}}{C_{33}(C_{11} + C_{12}) - 2C_{13}^2}, \quad S_{33} = \frac{C_{11} + C_{12}}{C_{33}(C_{11} + C_{12}) - 2C_{13}^2} \end{aligned} \quad (16)$$

The calculated results of S_{11} , S_{12} , S_{13} , S_{33} , and S_{44} for Ti_3Al under different pressures are presented in Table 3. The calculated results of Young's modulus, shear modulus, and Poisson's ratio on the prismatic and basal planes for Ti_3Al under different pressures are presented in Figure 8. It is clearly found that the values of $E_{(2\bar{1}0)}$, $E_{(010)}$, and $E_{(001)}$ on the prismatic and basal planes increase with pressure. The Young's modulus on the $(2\bar{1}0)$ and (010) prismatic planes are much smaller than the counterpart on the (001) basal plane, indicating the very significant anisotropic behavior of Ti_3Al under different pressures. Meanwhile, the difference between the prismatic planes $E_{(2\bar{1}0)}$ and $E_{(010)}$ and the basal plane $E_{(001)}$ increases with pressure, indicating that the elastic anisotropy of Ti_3Al increases with pressure. However, the shear modulus on the two prismatic planes are closed to the counterpart on the basal plane, and the same result occurs for Poisson's ratio.

Table 3. The elastic compliances S_{ij} (in $\times 10^{-3}\text{GPa}^{-1}$) of Ti_3Al under pressure up to 80 GPa.

P	S_{11}	S_{12}	S_{13}	S_{33}	S_{44}
0	7.07	-2.87	-1.13	4.9	16.74
10	6.01	-2.6	-0.901945	3.97	15.12
20	5.15	-2.17	-0.823186	3.55	14.24
30	4.71	-2.01	-0.804515	3.3	13.72
40	4.37	-1.86	-0.809706	3.15	13.48
50	4.14	-1.79	-0.790763	3.02	13.5
60	3.96	-1.75	-0.764448	2.85	13.64
70	3.80	-1.74	-0.722140	2.68	13.95
80	3.73	-1.8	-0.679304	2.51	14.33

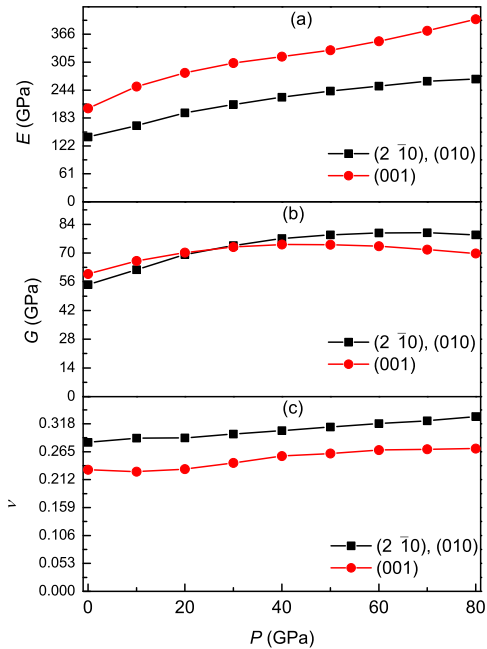


Figure 8. Young's modulus (a), shear modulus (b), and Poisson's ratio (c) on the $(2\bar{1}0)$, (010) , and (001) planes as a function of pressure for Ti_3Al .

An alternative method is the investigation of various anisotropic factors. The shear anisotropic factor for the $\{100\}$ planes between $\langle 011 \rangle$ and $\langle 010 \rangle$ directions is [31]

$$A_{\{100\}} = \frac{4C_{44}}{C_{11} + C_{33} - 2C_{13}} \quad (17)$$

For the $\{010\}$ planes between $\langle 211 \rangle$ and $\langle 001 \rangle$ directions, it is [31]

$$A_{\{010\}} = \frac{4C_{55}}{C_{22} + C_{33} - 2C_{23}} \quad (18)$$

For the $\{001\}$ planes between $\langle 110 \rangle$ and $\langle 120 \rangle$ directions, it is [31]

$$A_{\{001\}} = \frac{4C_{66}}{C_{11} + C_{22} - 2C_{12}} \quad (19)$$

For an isotropic material, the value of $A_{\{100\}}$, $A_{\{010\}}$, and $A_{\{001\}}$ must be unity. A deviation less than or greater than unity represents the degree of anisotropy. The calculated results of $A_{\{100\}}$, $A_{\{010\}}$, and $A_{\{001\}}$ for Ti_3Al under different pressures are presented in Figure 9. It is clearly seen that the values of $A_{\{100\}}$ and $A_{\{010\}}$ are significantly smaller than unity and decrease monotonously with pressure, whereas the value of $A_{\{001\}}$ under different pressures is always equal to unity. These results show that as pressure increases, the elastic anisotropy on the $\{100\}$ and $\{010\}$ planes of Ti_3Al increases, while the compound always exhibits isotropic behavior on the $\{001\}$ basal plane, which agrees with the general property of hexagonal materials.

The percentage anisotropy for the bulk modulus (A^B) and shear modulus (A^G) is given by [40]

$$A^B = \frac{B_V - B_R}{B_V + B_R} \times 100\%, \quad A^G = \frac{G_V - G_R}{G_V + G_R} \times 100\% \quad (20)$$

The universal anisotropy index (A^U) is given by [41]

$$A^U = \frac{B_V}{B_R} + 5 \frac{G_V}{G_R} - 6 \quad (21)$$

The scalar log-Euclidean anisotropy index (A^L) is given by [42]

$$A^L = \sqrt{[\ln(\frac{B_V}{B_R})]^2 + 5[\ln(\frac{G_V}{G_R})]^2} \quad (22)$$

For an isotropic material, the values of A^B , A^G , A^U , and A^L must be zero. A deviation greater than zero represents the degree of anisotropy. The calculated results of A^B , A^G , A^U , and A^L are also presented in Figure 9 for Ti₃Al under different pressures. It is clearly seen that as pressure increases, the value of A^B is almost kept at zero, while that of A^G increases approximately. At identical pressure, the value of A^B is significantly smaller than that of A^G . Similar to A^G , the values of A^U and A^L also increase approximately with pressure. The results indicate that the shear anisotropy of Ti₃Al is more significant than the compressibility anisotropy, and its elastic anisotropy is approximately enhanced with pressure.

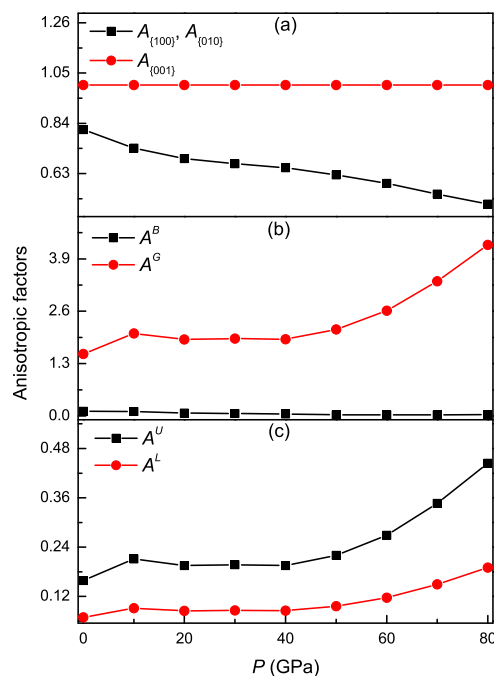


Figure 9. Shear anisotropic factors $A_{\{100\}}$, $A_{\{010\}}$, and $A_{\{001\}}$ (a), percentage anisotropy in compressibility A^B and shear A^G (b), the universal anisotropy index A^U and the log-Euclidean anisotropy index A^L (c) as a function of pressure for Ti₃Al.

3.5. Pressure-Dependent Acoustic and Related Properties

The pure longitudinal (v_l) and transverse (v_t) sound velocities in the [100] and [001] principal directions for hexagonal Ti₃Al can be calculated from the obtained constants C_{ij} s of a single crystal following the procedure of Brugger [43]. The sound velocities in the [100] direction are given by [44,45]

$$[100]v_l = \sqrt{\frac{C_{11} - C_{12}}{2\rho}}, \quad [010]v_{t1} = \sqrt{\frac{C_{11}}{\rho}}, \quad [001]v_{t2} = \sqrt{\frac{C_{44}}{\rho}} \quad (23)$$

and those in the [001] direction are given by [44,45]

$$[001]v_l = \sqrt{\frac{C_{33}}{\rho}}, \quad [100]v_{t1} = [010]v_{t2} = \sqrt{\frac{C_{44}}{\rho}} \quad (24)$$

where v_{t_1} and v_{t_2} correspond to the first and the second transverse modes, and ρ represents the mass density of the compound. Since these sound velocities are determined by the elastic constants, their anisotropic properties also reflect the elastic anisotropy in Ti_3Al . Additionally, the longitudinal (V_L) and transverse (V_T) sound velocities of polycrystal Ti_3Al can also be calculated from the obtained bulk modulus B and shear modulus G , which are given by [46]

$$V_L = \sqrt{\frac{3B + 4G}{3\rho}}, \quad V_T = \sqrt{\frac{G}{\rho}} \quad (25)$$

Further, the average sound velocity (V_M) can be calculated by [47]

$$V_M = \left[\frac{1}{3} \left(\frac{1}{V_L^3} + \frac{2}{V_T^3} \right) \right]^{-\frac{1}{3}} \quad (26)$$

The calculated results of longitudinal and transverse sound velocities for Ti_3Al under different pressures are presented in Figure 10. It is clearly seen that the values of $[100]v_l$, $[010]v_{t1}$, and $[001]v_l$ of a single crystal increase while those of $[001]v_{t2}$, $[100]v_{t1}$, and $[010]v_{t2}$ decrease with pressure, which is consistent with the variation trend of the corresponding elastic constants. Meanwhile, the value of V_L of the polycrystal also increases while those of V_T and V_M increase firstly and then decrease with pressure. Moreover, the value of $[100]v_l$ is much smaller than that of $[001]v_l$ at identical pressure, and the corresponding absolute difference increases with pressure. The results indicate that the anisotropy of sound velocity for Ti_3Al is very significant and increases with pressure.

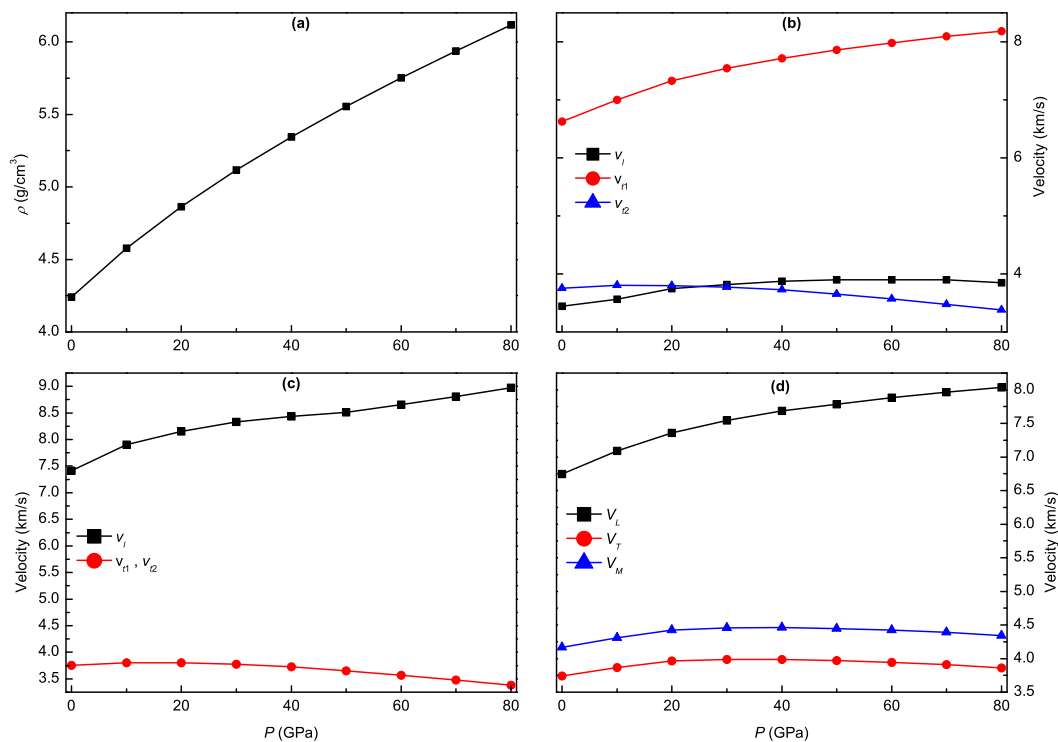


Figure 10. Mass density ρ (a), longitudinal and transverse sound velocities v_l , v_{t1} , and v_{t2} in the [100] (b) and [001] (c) principle directions, and polycrystalline longitudinal, transverse, and average sound velocities V_L , V_T , and V_M (d) as a function of pressure for Ti_3Al .

The minimum thermal conductivity is defined as an extreme value of the thermal conductivity decreasing with temperature. From the obtained Young's modulus and mass density, the minimum thermal conductivity (k_{min}) of Ti_3Al can be calculated according to Clarke's model [48]:

$$k_{min} = 0.87k_B \sqrt[3]{(\frac{n\rho N_A}{M})^2} \sqrt{\frac{E}{\rho}} \quad (27)$$

where k_B , n , N_A , and M are, in turn, the Boltzmann constant, total atoms per primitive cell, Avogadro's number, and relative molecular weight. However, the model averages the anisotropic elastic stiffness of a crystal. To calculate precisely the minimum thermal conductivity of the crystal with elastic anisotropy, the model was further modified by Liu et al. [49] as

$$k_{min} = \{\frac{1}{3}[2(\frac{1}{2+2\nu})^{-\frac{3}{2}} + (\frac{1}{3-6\nu} + \frac{2}{3+3\nu})^{-\frac{3}{2}}]\}^{-\frac{1}{3}} k_B \sqrt[3]{(\frac{n\rho N_A}{M})^2} \sqrt{\frac{E}{\rho}} \quad (28)$$

Figure 11 shows the pressure dependence of minimum thermal conductivity for Ti_3Al . It is clearly observed that the value of k_{min} obtained from the two models increases monotonously with pressure. At the same pressure, the k_{min} value calculated by the modified Clarke's model is significantly smaller than that calculated by Clarke's model. This shows that the minimum thermal conductivity of Ti_3Al is markedly reduced after considering its elastic anisotropy.

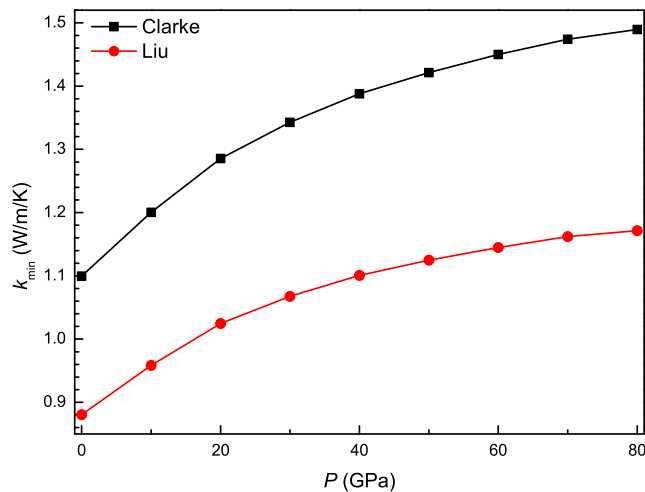


Figure 11. Minimum thermal conductivities as a function of pressure for Ti_3Al .

In addition to minimum thermal conductivity, the Debye temperature (Θ_D) of Ti_3Al can be calculated from the average sound velocity of its polycrystal by [47]

$$\Theta_D = \frac{h}{k_B} [\frac{3n}{4\pi} (\frac{N_A \rho}{M})]^{\frac{1}{3}} V_M \quad (29)$$

where the parameters h , k_B , n , N_A , and M are, in turn, the Plank constant, the Boltzmann constant, number of atoms in the molecule formula, Avogadro's number, and molecular weight. Figure 12 show the pressure dependence of Debye temperature for Ti_3Al . It is clearly found that the value of Θ_D increases monotonously with pressure and exhibits a change trend similar to the minimum thermal conductivity, following the Callaway–Debye theory [50]. Experimentally, the Debye temperature of Ti_3Al was determined as 495 K from specific heat measurements [51] and 478 K from the single-crystal X-ray diffraction pattern [52], which agree well with our calculated value of 485.16 K at zero pressure.

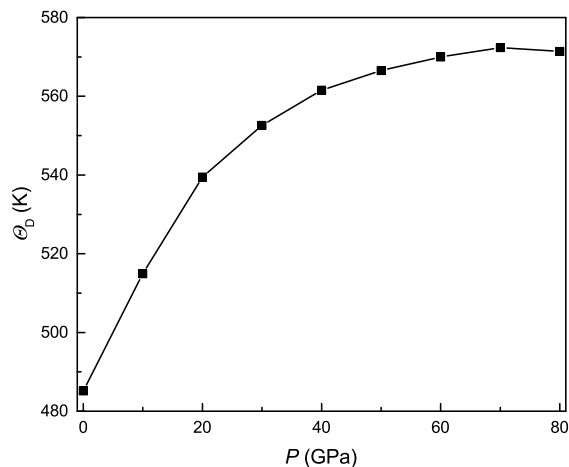


Figure 12. Debye temperature as a function of pressure for Ti_3Al .

4. Conclusions

The elastic constants and their related properties, such as elastic moduli, Poisson's ratio, anisotropic factor, acoustic velocity, minimum thermal conductivity, and Debye temperature, were investigated for hexagonal Ti_3Al under different pressures up to 80 GPa by using first-principles calculations. The present results at zero pressure are in good agreement with the previous experimental and theoretical values. The resistance to compression along the c axis is better than along the a axis under each pressure. According to the mechanical stability criteria under isotropic pressure, the hexagonal structure of Ti_3Al is judged to be mechanically stable under pressures up to 71.4 GPa. The bulk modulus, shear modulus, Young's modulus, Poisson's ratio, Cauchy pressures, and hardness were calculated, which show that the ductility of Ti_3Al is improved with pressure. The linear bulk modulus, the direction-dependent Young's modulus, shear modulus, and Poisson's ratio, the shear anisotropic factors, the percentage anisotropy of bulk modulus and shear modulus, and the universal and the log-Euclidean anisotropy indexes were also calculated, which show that the elastic anisotropy of Ti_3Al is very significant and increases with pressure. Moreover, the significant anisotropy of sound velocity for Ti_3Al increases with pressure. The obtained minimum thermal conductivity and Debye temperature increase with pressure.

Author Contributions: Conceptualization, X.Z. and Y.W.; Methodology, X.Z. and Y.W.; Software, Y.W.; Validation, Y.Y., Z.H. and L.S.; Formal analysis, Y.Y., Z.H. and L.S.; Investigation, X.Z. and Y.W.; Resources, L.S. and Y.W.; Data curation, X.Z., Y.Y. and Z.H.; Writing—original draft preparation, X.Z.; Writing—review and editing, R.P. and Y.W.; Visualization, X.Z. and Y.W.; Supervision, Y.W. and R.P.; Project administration, Y.W.; Funding acquisition, Y.W. and L.S.

Funding: This research was funded by National Natural Science Foundation of China (Nos. 51661013, 51601146).

Acknowledgments: This project was granted technical support from Mei Wei in National Supercomputing center in Shenzhen.

Conflicts of Interest: The authors declare no conflict of interest.

References

- Ravindran, P.; Fast, L.; Korzhavyi, P.A.; Johansson, B.; Wills, J.; Eriksson, O. Density functional theory for calculation of elastic properties of orthorhombic crystals: Application to TiSi_2 . *J. Appl. Phys.* **1998**, *84*, 4891–4904. [[CrossRef](#)]
- Djanarthany, S.; Viala, J.C.; Bouix, J. An overview of monolithic titanium aluminides based on Ti_3Al and TiAl . *Mater. Chem. Phys.* **2001**, *72*, 301–319. [[CrossRef](#)]
- Court, S.A.; Löfvander, J.P.A.; Loretto, M.H.; Fraser, H.L. The influence of temperature and alloying additions on the mechanisms of plastic deformation of Ti_3Al . *Philos. Mag. A* **1990**, *61*, 109–139. [[CrossRef](#)]
- Lipsitt, H.A.; Shechtman, D.; Schafrik, R. The deformation and fracture of TiAl at elevated temperatures. *Metall. Trans. A* **1975**, *6*, 1991–1996. [[CrossRef](#)]

5. Umakoshi, Y.; Nakano, T.; Sumimoto, K.; Maeda, Y. Plastic anisotropy of Ti_3Al single crystals. *Mater. Res. Soc. Symp. Proc.* **1993**, *288*, 441–446. [[CrossRef](#)]
6. Sahu, P.C.; Chandra, N.V.; Shekar, C.; Yousuf, M.; Rajan, K.G. Implications of a pressure induced phase transition in the search for cubic Ti_3Al . *Phys. Rev. Lett.* **1997**, *78*, 1054–1057. [[CrossRef](#)]
7. Rajagopalan, M.; Sahu, P.C.; Shekar, C.; Yousuf, M.; Rajan, K.G. Structural phase stability of Ti_3Al under high pressure. *Int. J. Mod. Phys. B* **1999**, *13*, 841–845. [[CrossRef](#)]
8. Dubrovinskaia, N.A.; Vennström, M.; Abrikosov, I.A.; Ahuja, R.; Ravindran, P.; Andersson, Y.; Eriksson, O.; Dmitriev, V.; Dubrovinsky, L.S. Absence of a pressure-induced structural phase transition in Ti_3Al up to 25 GPa. *Phys. Rev. B* **2000**, *63*, 024106. [[CrossRef](#)]
9. Zhang, C.; Hou, H.; Zhao, Y.; Yang, X.; Guo, Y. First-principles study on structural, elastic thermal properties of γ - $TiAl$ and α_2 - Ti_3Al phases in TiAl-based alloy under high pressure. *Int. J. Mod. Phys. B* **2017**, *31*, 1750079. [[CrossRef](#)]
10. Kresse, G.; Hafner, J. Ab initio molecular dynamics for open-shell transition metals. *Phys. Rev. B* **1993**, *48*, 13115–13118. [[CrossRef](#)]
11. Kresse, G.; Furthmüller, J. Efficiency of ab-initio total energy calculations for metals and semiconductors using a plane-wave basis set. *Comput. Mater. Sci.* **1996**, *6*, 15–50. [[CrossRef](#)]
12. Kresse, G.; Furthmüller, J. Efficient iterative schemes for ab initio total-energy calculations using a plane-wave basis set. *Phys. Rev. B* **1996**, *54*, 11169–11186. [[CrossRef](#)]
13. Blöchl, P.E. Projector augmented-wave method. *Phys. Rev. B* **1994**, *50*, 17953–17979. [[CrossRef](#)]
14. Kresse, G.; Joubert, D. From ultrasoft pseudopotentials to the projector augmented-wave method. *Phys. Rev. B* **1999**, *59*, 1758–1775. [[CrossRef](#)]
15. Perdew, J.P.; Burke, K.; Ernzerhof, M. Generalized gradient approximation made simple. *Phys. Rev. Lett.* **1996**, *77*, 3865–3868. [[CrossRef](#)] [[PubMed](#)]
16. Perdew, J.P.; Burke, K.; Ernzerhof, M. Generalized gradient approximation made simple [Phys. Rev. Lett. 77, 3865 (1996)]. *Phys. Rev. Lett.* **1997**, *78*, 1396. [[CrossRef](#)]
17. Monkhorst, H.J.; Pack, J.D. Special points for Brillouin-zone integrations. *Phys. Rev. B* **1976**, *13*, 5188–5192. [[CrossRef](#)]
18. Hafner, R.J. Materials simulations using VASP—A quantum perspective to materials science. *Comput. Phys. Commun.* **2007**, *177*, 6–13. [[CrossRef](#)]
19. Le Page, Y.; Saxe, P. Symmetry-general least-squares extraction of elastic data for strained materials from ab initio calculations of stress. *Phys. Rev. B* **2002**, *65*, 104104. [[CrossRef](#)]
20. Wu, X.; Vanderbilt, D.; Hamann, D.R. Systematic treatment of displacements, and electric fields in density-functional perturbation theory. *Phys. Rev. B* **2005**, *72*, 035105. [[CrossRef](#)]
21. Tanaka, K.; Koiwa, M. Single-crystal elastic constants of intermetallic compounds. *Intermetallics* **1996**, *4*, S29–S39. [[CrossRef](#)]
22. Wei, Y.; Zhang, Y.; Lu, G.H.; Xu, B. Site preference and elastic properties of α_2 - Ti_3Al with oxygen impurity: A first-principles study. *Int. J. Mod. Phys. B* **2010**, *24*, 2749–2755. [[CrossRef](#)]
23. Liu, Y.L.; Liu, L.M.; Wang, S.Q.; Ye, H.Q. First-principles study of shear deformation in TiAl and Ti_3Al . *Intermetallics* **2007**, *15*, 428–435. [[CrossRef](#)]
24. Music, D.; Schneider, J.M. Effect of transition metal additives on electronic structure and elastic properties of TiAl and Ti_3Al . *Phys. Rev. B* **2006**, *74*, 174110–174114. [[CrossRef](#)]
25. Fu, C.L.; Zou, J.; Yoo, M.H. Elastic constants and planar fault energies of Ti_3Al , and interfacial energies at the $Ti_3Al/TiAl$ interface by first-principles calculations. *Scr. Metall. Mater.* **1995**, *33*, 885–891. [[CrossRef](#)]
26. Pearson, W.B. *A Handbook of Lattice Spacing and Structure of Metals and Alloys*; Pergamon: Oxford, UK, 1987; pp. 1–2.
27. Mouhat, F.; Coudert, F.X. Necessary and sufficient elastic stability conditions in various crystal systems. *Phys. Rev. B* **2014**, *90*, 224104. [[CrossRef](#)]
28. Sinko, G.V.; Smirnow, N.A. Ab initio calculations of elastic constants and thermodynamic properties of bcc, fcc, and hcp Al crystals under pressure. *J. Phys. Condens. Matter* **2002**, *14*, 6989–7005.
29. Hill, R. The elastic behaviour of a crystalline aggregate. *Proc. Phys. Soc. A* **1952**, *65*, 349–354. [[CrossRef](#)]
30. Tao, X.; Yang, J.; Xi, L.; Ouyang, Y. First-principles investigation of the thermo-physical properties of Ca_3Si_4 . *J. Solid State Chem.* **2012**, *194*, 179–187. [[CrossRef](#)]

31. Mao, P.; Yu, B.; Liu, Z.; Wang, F.; Ju, Y. First-principles investigation on mechanical, electronic, and thermodynamic properties of Mg₂Sr under high pressure. *J. Appl. Phys.* **2015**, *117*, 115903. [[CrossRef](#)]
32. Voigt, W. *Lehrbuch der Kristallphysik*; Taubner: Leipzig, Germany, 1928.
33. Reuss, A. Calculation of the flow limits of mixed crystals on the basis of the plasticity of monocrystals. *Z. Angew. Math. Mech.* **1929**, *9*, 49–58. [[CrossRef](#)]
34. Pugh, S.F. Relations between the elastic moduli and the plastic properties of polycrystalline pure metals. *Philos. Mag.* **1954**, *45*, 823–843. [[CrossRef](#)]
35. Frantsevich, I.N.; Voronov, F.F.; Bokuta, S.A. *Elastic Constants and Elastic Moduli of Metals and Insulators Handbook*; Frantsevich, I.N., Ed.; Naukova Dumka: Kiev, Ukraine, 1983; pp. 60–180.
36. Pettifor, D.G. Theoretical predictions of structure and related properties of intermetallics. *Mater. Sci. Technol.* **1992**, *8*, 345–349. [[CrossRef](#)]
37. Chen, X.Q.; Niu, H.; Li, D.; Li, Y. Intrinsic correlation between hardness and elasticity in polycrystalline materials and bulk metallic glasses. *Intermetallics* **2011**, *19*, 1275–1281. [[CrossRef](#)]
38. Ravindran, P.; Vajeeston, P.; Vidya, R.; Kjekshus, A.; Fjellvåg, H. Detailed electronic structure studies on superconducting MgB₂ and related compounds. *Phys. Rev. B* **2001**, *64*, 224509. [[CrossRef](#)]
39. Pabst, W.; Gregorova, E. Effective elastic properties of alumina-zirconia composite ceramics—Part 2. Micromechanical modeling. *Ceram. Silik.* **2004**, *48*, 14–23.
40. Chung, D.H.; Buessem, W.R. The elastic anisotropy of crystals. *J. Appl. Phys.* **1967**, *38*, 2010–2012. [[CrossRef](#)]
41. Ranganathan, S.I.; Ostoja-Starzewski, M. Universal elastic anisotropy index. *Phys. Rev. Lett.* **2008**, *101*, 055504. [[CrossRef](#)] [[PubMed](#)]
42. Kube, C.M. Elastic anisotropy of crystals. *AIP Adv.* **2016**, *6*, 095209. [[CrossRef](#)]
43. Brugger, K. Determination of third-order elastic coefficients in crystals. *J. Appl. Phys.* **1965**, *36*, 768–773. [[CrossRef](#)]
44. Duan, Y.H.; Sun, Y.; Peng, M.J.; Zhou, S.G. Anisotropic elastic properties of the Ca–Pb compounds. *J. Alloys Compd.* **2014**, *595*, 14–21. [[CrossRef](#)]
45. Sun, L.; Gal, Y.; Xiao, B.; Li, Y.; Wang, G. Anisotropic elastic and thermal properties of titanium borides by first-principles calculations. *J. Alloys Compd.* **2013**, *579*, 457–467. [[CrossRef](#)]
46. Schreiber, E.; Anderson, O.L.; Soga, N. *Elastic Constants and Their Measurements*; McGraw: New York, NY, USA, 1973.
47. Anderson, O.L. A simplified method for calculating the Debye temperature from elastic constants. *J. Phys. Chem. Solids* **1963**, *24*, 909–917. [[CrossRef](#)]
48. Clarke, D.R. Materials selection guidelines for low thermal conductivity thermal barrier coatings. *Surf. Coat. Technol.* **2003**, *163–164*, 67–74. [[CrossRef](#)]
49. Liu, B.; Wang, J.Y.; Li, F.Z.; Zhou, Y.C. Theoretical elastic stiffness, structural stability and thermal conductivity of La₂T₂O₇ (*T* = Ge, Ti, Sn, Zr, Hf) pyrochlore. *Acta Mater.* **2010**, *58*, 4369–4377. [[CrossRef](#)]
50. Callaway, J. Model for lattice thermal conductivity at low temperatures. *Phys. Rev.* **1959**, *113*, 1046–1051. [[CrossRef](#)]
51. Collings, E.W.; Ho, J.C. *Science, Technology and Application of Titanium*; Jaffee, R.I., Promisel, N.E., Eds.; Pergamon: London, UK, 1970; pp. 331–347.
52. Gehlen, P.C. *Science, Technology and Application of Titanium*; Jaffee, R.I., Promisel, N.E., Eds.; Pergamon: London, UK, 1970; pp. 349–357.



© 2018 by the authors. Licensee MDPI, Basel, Switzerland. This article is an open access article distributed under the terms and conditions of the Creative Commons Attribution (CC BY) license (<http://creativecommons.org/licenses/by/4.0/>).